J|A|C|S ARTICLES

Published on Web 01/06/2010

Large All-Hydrocarbon Spoked Wheels of High Symmetry: Modular Synthesis, Photophysical Properties, and Surface Assembly

Dennis Mössinger,[†,‡] Debangshu Chaudhuri,[‡] Tibor Kudernac,[§] Shengbin Lei,[§] Steven De Feyter,[*,§] John M. Lupton,[*,‡] and Sigurd Höger[*,†]

Kekulé-Institut für Organische Chemie und Biochemie, Rheinische Friedrich-Wilhelms-Universität Bonn, Gerhard-Domagk-Strasse 1, 53121 Bonn, Germany, Department of Physics and Astronomy, University of Utah, Salt Lake City, Utah 84112, and Department of Chemistry, Laboratory of Photochemistry and Spectroscopy, and Institute for Nanoscale Physics and Chemistry, Katholieke Universiteit Leuven, Celestijnenlaan 200-F, 3001 Leuven, Belgium

Received October 30, 2009; E-mail: hoeger@uni-bonn.de; lupton@physics.utah.edu; steven.defeyter@chem.kuleuven.be

Abstract: In a convergent modular synthesis, a very efficient pathway to shape-persistent molecular spoked wheels has been developed and applied according to the covalent-template concept. The structurally defined two-dimensional (2D) oligo(phenylene-ethynylene-butadiynylene)s (OPEBs) presented here are about 8 nm sized hydrocarbons of high symmetry. 48 alkyl chains attached to the molecular plane (hexyl and hexadecyl, respectively) guarantee a high solubility of the compounds. The structure and uniformity of these defined, stable, D_{6h} symmetrical compounds is verified by MALDI-MS, GPC analysis, and high-temperature (HT) ^{1}H and ^{13}C NMR. Detailed photophysical measurements of nonaggregated molecules in solution (as confirmed by dynamic light scattering (DLS)) focus on the identification of chromophores by comparison with suitable model compounds. Moreover, time-resolved measurements including fluorescence lifetime and depolarization support the chromophore assignment and reveal the occurrence of intramolecular energy transfer. Scanning tunneling microscope (STM) characterization at the solid/liquid interface demonstrates the efficient self-assembly of the OPEBs into hexagonal 2D crystalline layers with a periodicity determined by both the size of the OPEB backbone and the length of peripheral side chains. Atomic force microscope (AFM) studies show a very different assembly behavior of the two spoked wheel molecules, on both graphite and mica. While the hexyl-substituted wheel can form stacked superstructures, hexadecyl groups prevent any ordering in the film aside from the monolayer directly in contact with the surface.

Introduction

Large two-dimensional (2D) shape-persistent, carbon-rich molecules of defined constitution, size, and shape have gained increasing importance in material science. 2D nanostructures fulfilling these criteria exhibit interesting properties such as 2D crystallinity on surfaces,[1−7] liquid crystallinity,[8−10] and intriguing photophysical features.[11−15] Moreover, shape-persistent organic structures are expected to show reinforcement effects in nanocomposite materials as affirmed recently by the successful use of carbon nanotubes (CNTs) as rigid components in polymer composites.[16,17]

[†] Rheinische Friedrich-Wilhelms-Universität Bonn.
[‡] University of Utah.
[§] Katholieke Universiteit Leuven.

(1) Samori, P.; Severin, N.; Simpson, C. D.; Müllen, K.; Rabe, J. P. *J. Am. Chem. Soc.* **2002**, *124*, 9454–9457.
(2) De Feyter, S.; De Schryver, F. *Top. Curr. Chem.* **2005**, *258*, p 205–255.
(3) Hermann, B. A.; Scherer, L. J.; Housecroft, C. E.; Constable, E. C. *Adv. Funct. Mater.* **2006**, *16*, 221–235.
(4) Pan, G.-B.; Cheng, X.-H.; Höger, S.; Freyland, W. *J. Am. Chem. Soc.* **2006**, *128*, 4218–4219.
(5) Mena-Osteritz, E.; Bäuerle, P. *Adv. Mater.* **2006**, *18*, 447–451.
(6) Lei, S.; Surin, M.; Tahara, K.; Adisoejoso, J.; Lazzaroni, R.; Tobe, Y.; Feyter, S. D. *Nano Lett.* **2008**, *8*, 2541–2546.
(7) Adisoejoso, J.; Tahara, K.; Okuhata, S.; Lei, S.; Tobe, Y.; De Feyter, S. *Angew. Chem., Int. Ed.* **2009**, *48*, 7353–7357.
(8) Zhang, J.; Moore, J. S. *J. Am. Chem. Soc.* **1994**, *116*, 2655–2656.
(9) Höger, S.; Cheng, X. H.; Ramminger, A.-D.; Enkelmann, V.; Rapp, A.; Mondeshki, M.; Schnell, I. *Angew. Chem., Int. Ed.* **2005**, *44*, 2801–2805.
(10) Wu, J.; Pisula, W.; Müllen, K. *Chem. Rev.* **2007**, *107*, 718–747.
(11) Schmidt-Mende, L.; Fechtenkötter, A.; Müllen, K.; Moons, E.; Friend, R. H.; MacKenzie, J. D. *Science* **2001**, *293*, 1119–1122.
(12) Song, H.-E.; Kirmaier, C.; Schwartz, J. K.; Hindin, E.; Yu, L.; Bocian, D. F.; Lindsey, J. S.; Holten, D. *J. Phys. Chem. B* **2006**, *110*, 19131–19139.
(13) Song, H.-E.; Kirmaier, C.; Schwartz, J. K.; Hindin, E.; Yu, L.; Bocian, D. F.; Lindsey, J. S.; Holten, D. *J. Phys. Chem. B* **2006**, *110*, 19121–19130.
(14) Kenji, K.; Liudmil, A.; Satoru, Y.; Koji, O.; Takashi, Y.; Kazukuni, T.; Akiko, I.; Motohiro, S.; Yoshito, T. *ChemPhysChem* **2007**, *8*, 2671–2677.
(15) Becker, K.; Fritzsche, M.; Höger, S.; Lupton, J. M. *J. Phys. Chem. B* **2008**, *112*, 4849–4853.
(16) Loiseau, A.; Tassin, J.-F. *Macromolecules* **2006**, *39*, 9185–9191.

 10.1021/ja909229y

Scheme 1. Star-Shaped Dodeca-acetylene Precursor **1** and Proof-of-Principle Spoked Wheel **2**[a]

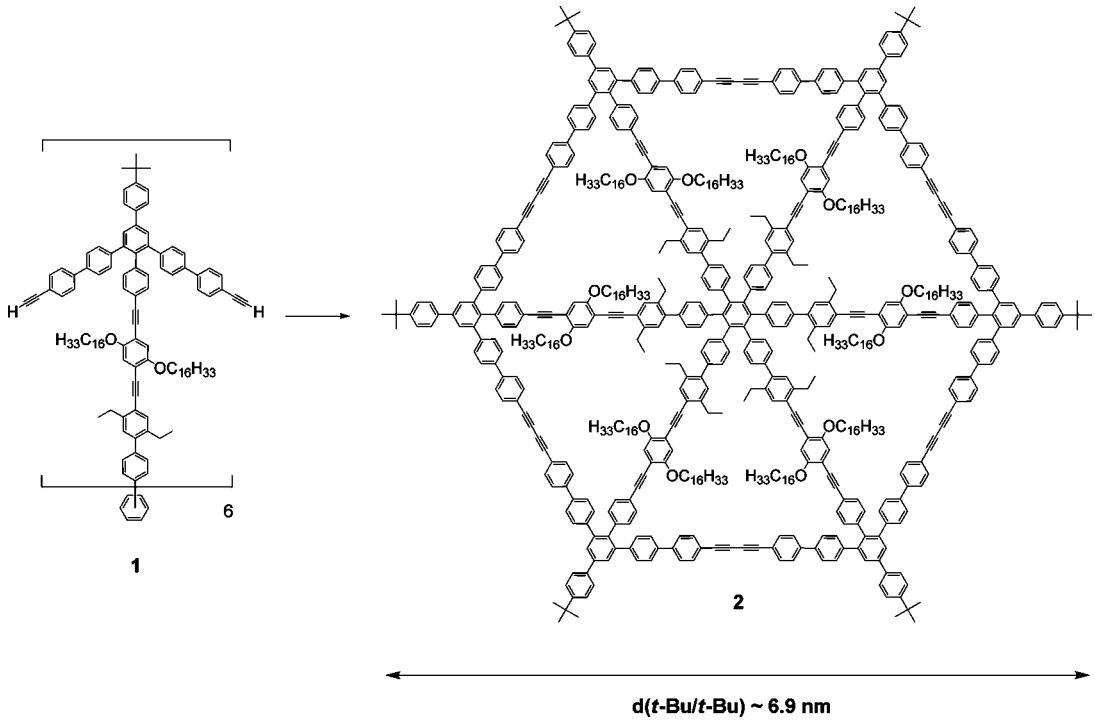

[a] Estimation of the molecular diameter performed with Wavefunction Spartan '08.

Recently, we described all-covalent molecular spoked wheels as large defined organic compounds beyond the 5 nm range.[18] In contrast to carbon-rich scaffolds such as graphene, graphyne, graphdiyne, and the respective cutouts,[19] these molecules do not rely on a specific idealized structure. The pursuit of these structures is on the one hand driven by scientific curiosity: demonstration of the synthetic feasibility of such large compounds along with the control over solubility. On the other hand, we aim at creating rigid organo-based materials for potential composite applications.

Just as shape-persistent macrocycles, spoked wheel structures allow the introduction of functionality at the perimeter as well as above and below the molecular plane. Although shape-persistent macrocycles tend to pack in flat (2D) arrangements on surfaces, single crystal structures[9,20,21] and molecular dynamics (MD) simulations[22,23] reveal considerable deviations from the planar conformation. By contrast, molecular spoked wheels have been designed as reinforced (strutted) macrocycles and combine favorable properties both from large disk-shaped polycyclic aromatic hydrocarbons (PAHs) (with shape-persistence, strict planarity, and a high degree of symmetry) and from conventional macrocycles (with solubility, ease of characterization, and the potential to introduce functional groups in the molecular plane and at the periphery). Columnar stacking, as observed for PAHs, should be successfully suppressed due to solubilizing chains orthogonal to the molecular plane. Beside some known covalent approaches,[24,25] most spoked wheel structures published so far were supramolecular complexes consisting of macrocyclic rims and multidentate, star-shaped interior scaffolds.[26−30] In most cases, these scaffolds have been utilized to facilitate cyclization or study the complex formation,[30,31] in part along with light-harvesting behavior.[13,28,32]

We demonstrated that large, strutted macrocycles are accessible in a covalent template approach: in a convergent synthesis, six preformed spoke/rim modules are coupled to a hexaiodo hub affording a star-shaped precursor molecule with 12 terminal acetylene units (**1**, Scheme 1). In an intramolecular reaction, adjacent acetylenes dimerize and form six defined butadiyne bridges. This means that the precursor contains its own covalently linked template, which remains bound inside the molecular spoked wheel (Scheme 1). The proof-of-principle

(17) Beigbeder, A.; Linares, M.; Devalckenaere, M.; Degée, P.; Claes, M.; Beljonne, D.; Lazzaroni, R.; Dubois, P. *Adv. Mater.* **2008**, *20*, 1003–1007.
(18) Mössinger, D.; Hornung, J.; Lei, S.; De Feyter, S.; Höger, S. *Angew. Chem., Int. Ed.* **2007**, *46*, 6802–6806.
(19) Diederich, F. *Nature* **1994**, *369*, 199–207.
(20) Höger, S.; Enkelmann, V. *Angew. Chem., Int. Ed. Engl.* **1996**, *34*, 2713–2716.
(21) Höger, S.; Morrison, D. L.; Enkelmann, V. *J. Am. Chem. Soc.* **2002**, *124*, 6734–6736.
(22) Ziegler, A.; Mamdouh, W.; Ver Heyen, A.; Surin, M.; Uji-i, H.; Abdel-Mottaleb, M. M. S.; De Schryver, F. C.; De Feyter, S.; Lazzaroni, R.; Höger, S. *Chem. Mater.* **2005**, *17*, 5670–5683.
(23) Lei, S.; Ver Heyen, A.; De Feyter, S.; Surin, M.; Lazzaroni, R.; Rosenfeldt, S.; Ballauff, M.; Lindner, P.; Mössinger, D.; Höger, S. *Chem.-Eur. J.* **2009**, *15*, 2518–2535.
(24) Marsden, J. A.; O'Connor, M. J.; Haley, M. M. *Org. Lett.* **2004**, *6*, 2385–2388.
(25) Bedard, T. C.; Moore, J. S. *J. Am. Chem. Soc.* **1995**, *117*, 10662–10671.
(26) Hoffmann, M.; Kärnbratt, J.; Chang, M.-H.; Herz, L. M.; Albinsson, B.; Anderson, H. L. *Angew. Chem., Int. Ed.* **2008**, *47*, 4993–4996.
(27) McCallien, D. W. J.; Sanders, J. K. M. *J. Am. Chem. Soc.* **1995**, *117*, 6611–6612.
(28) Jung, S.-H.; Pisula, W.; Rouhanipour, A.; Räder, H. J.; Jacob, J.; Müllen, K. *Angew. Chem., Int. Ed.* **2006**, *45*, 4685–4690.
(29) Tomizaki, K.-y.; Yu, L.; Wei, L.; Bocian, D. F.; Lindsey, J. S *J. Org. Chem.* **2003**, *68*, 8199–8207.
(30) Rucareanu, S.; Schuwey, A.; Gossauer, A. *J. Am. Chem. Soc.* **2006**, *128*, 3396–3413.
(31) Hoffmann, M.; Wilson, C. J.; Odell, B.; Anderson, H. L. *Angew. Chem., Int. Ed.* **2007**, *46*, 3122–3125.
(32) Chang, M.-H.; Hoffmann, M.; Anderson, H. L.; Herz, L. M. *J. Am. Chem. Soc.* **2008**, *130*, 10171–10178.

Scheme 2. Target Structures **3a** and **3b**: All-Hydrocarbon Spoked Wheels of High Symmetry[a]

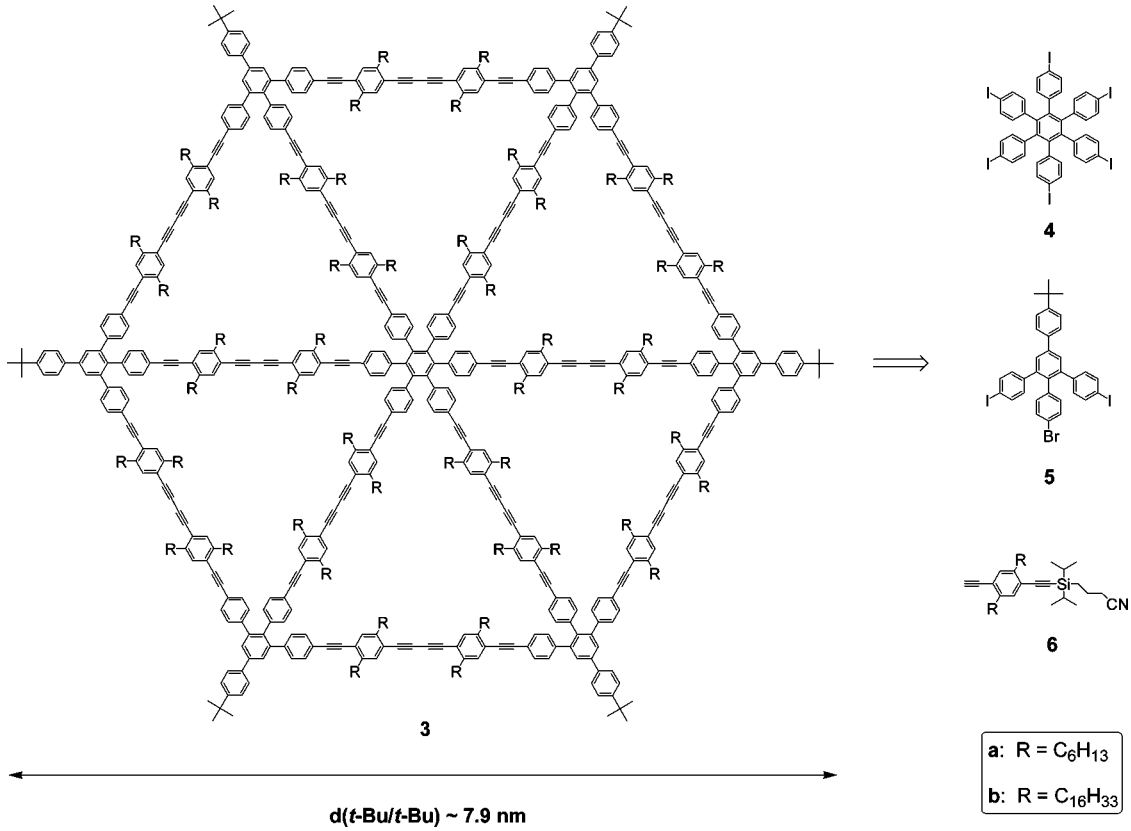

[a] Estimation of the molecular diameter performed with Wavefunction Spartan '08.

wheel **2** was moderately soluble due to 12 orthogonal side groups attached at the spokes. Its structure has been confirmed by MALDI MS, ^{1}H NMR, molecular modeling, small-angle neutron scattering (SANS), scanning-tunneling microscopic (STM), and atomic force microscopic (AFM) investigations. As intended, the reinforcement of the macrocyclic rim by diagonal spokes (or vice versa) caused a huge gain in rigidity.[23] Because of their regular 6-fold symmetric structure consisting of formal repeating units, we denoted the wheel molecules as "2D oligomers".[33,34] Despite their 7 nm size, individual molecules of the prototype **2** could be accommodated inside the voids of a honeycomb-like dehydrobenzo[12]annulene host network on HOPG, thus allowing the observation of rotational and adsorption/desorption dynamics of "isolated" molecules.[35]

The successful template-directed cyclization of **1** to **2** prompted us to investigate this concept on similar systems. However, to perform detailed spectroscopic studies (UV−vis), we searched for a geometry with a higher degree of symmetry, yet accessible in a more facile synthesis. Here, we present an efficient synthesis toward pure hydrocarbon spoked wheels, which is based on a simple modular approach (Scheme 2). With a limited number of building blocks and reduced synthetic effort, a compound with a diameter of nearly 8 nm is obtained. 48 alkyl chains attached orthogonally to the molecular plane considerably improve the solubility of the new systems compared to the prototype **2**. To stress the influence of the alkyl chain length on surface affinities and aggregation tendencies, two representatives with hexyl (**3a**) and hexadecyl groups (**3b**) have been synthesized (Scheme 2).

The wheel's highly symmetrical structure, originating from identical linear segments employed both as spokes and as rim segments, and a regular substitution pattern, provides simple UV−vis absorption and emission spectra. Thus, this system permits the construction of simple model compounds to allocate different chromophores within the wheel and the noncyclic precursors. These models can be applied to study basic (static and time-resolved) photophysical properties of spoked wheel compounds in general. In addition, the organization of **3** on solid surfaces as a function of the alkyl group length is investigated by means of STM and AFM.

Synthesis

As compared to the previously described synthesis of the prototype **2**, the new synthetic approach toward **3** has several advantages. First, the number of 6-fold transformations has been reduced and the synthetic toolbox of the critical several-fold C−C coupling steps was limited to high-yield Sonogashira−Hagihara and Glaser reactions.[36] The hub, previously synthesized in five steps including two 6-fold transformations, has been replaced by **4**, which is available in one step and good yields through iodination of hexaphenylbenzene with [bis(trifluoroacetoxy)iodo]benzene (PIFA) (Scheme 3).[37] Furthermore, pre-

(33) Jenkins, A. D.; Kratochvíl, P.; Stepto, R. F. T.; Suter, U. W. *Pure Appl. Chem.* **1996**, *68*, 2287–2311.
(34) Sakamoto, J.; van Heijst, J.; Lukin, O.; Schlüter, A. D. *Angew. Chem., Int. Ed.* **2009**, *48*, 1030–1069.
(35) Tahara, K.; Lei, S.; Mössinger, D.; Kozuma, H.; Inukai, K.; van der Auweraer, M.; De Schryver, F. C.; Höger, S.; Tobe, Y.; De Feyter, S. *Chem. Commun.* **2008**, 3897–3899.
(36) The several-fold Suzuki coupling steps could not be optimized further than 90% conversion per bond (52% in total).
(37) Kobayashi, K.; Kobayashi, N.; Ikuta, M.; Therrien, B.; Sakamoto, S.; Yamaguchi, K. *J. Org. Chem.* **2005**, *70*, 749–752.

Scheme 3. Module Construction, Convergent Assembly, and Template-Directed Cyclization[a]

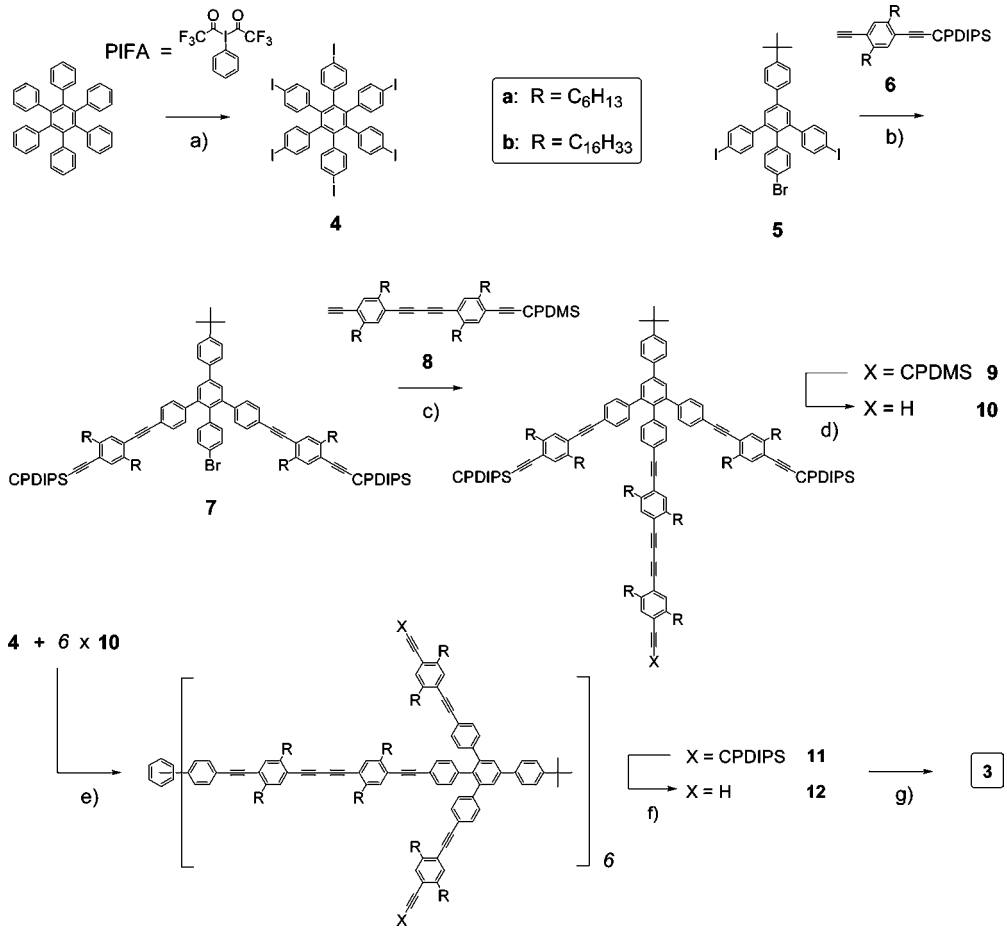

[a] (a) I_2, PIFA, CH_2Cl_2, room temperature, 36 h, recryst. *n*-hexane/$CHCl_3$ (1:1, v/v), 74%; (b) [$PdCl_2(PPh_3)_2$], CuI, PPh_3, piperidine, THF, room temperature, 16 h, **7a**, 89%, **7b**, 98%; (c) $Na_2[PdCl_4]$, CuI, P(*t*-Bu)$_3$, HN(*i*-Pr)$_2$, 80 °C, 16 h, **9a**, 90%, **9b**, 88%; (d) K_2CO_3, THF, MeOH, room temperature, 2 h, **10a**, 99%, **10b**, 96%; (e) [$PdCl_2(PPh_3)_2$], CuI, PPh_3, piperidine, 80 °C, 16 h, **11a**, 73%, **11b**, 78%; (f) excess TBAF═[NBu_4]F, 1.0 M in THF, 5% H_2O, 0−20 °C, 3 h, **12a**, 86%, **12b**, 92%; (g) **3a**, CuCl, $CuCl_2$, pyridine, DBU (2%, v/v), 50 °C, 4 d, 75%; **3b**, [$PdCl_2(PPh_3)_2$], CuI, I_2, THF, HN(*i*-Pr)$_2$, 50 °C, 3 d, recycling GPC separation, 64%.

fabricated bisacetylene rods of defined length were used to construct the spoke and rim segments.[38,39] These bisacetylenes can be statistically monoprotected[40] either with the stable (3-cyanopropyl)diisopropylsilyl (CPDIPS)[41] protective group or with the more labile (3-cyanopropyl)dimethylsilyl (CPDMS)[42] protective group to give versatile linear building blocks such as **6** and **8**. In general, polar acetylene protective groups dramatically simplify chromatographic separations of otherwise nonpolar (hydrocarbon) coupling products.[43]

As pointed out in Schemes 2 and 3, both spoked wheels **3a** and **3b** rely on the same building blocks **4** and **5**, but differ in building blocks **6** and **8**, which either bear hexyl (**a**) or hexadecyl (**b**) groups. The reaction sequence starts with the assembly of the spoke/rim modules. Because the pyrylium salt route[44,45] still marks one of most efficient pathways to functionalized *m*-terphenyl cornerpieces,[46] we retained the synthesis of the bromodiiodo compound **5** (two steps, 27% yield).[23] Using standard Sonogashira conditions ([$PdCl_2(PPh_3)_2$], CuI, piperidine, THF) at room temperature, the iodo functionalities of **5** were selectively coupled with the monoprotected bisacetylenes **6** (Scheme 3).[47] **7** was obtained in very good yields (89−98%) and could be easily separated from the byproducts due to its polar protective groups. In the next step, the complete spoke should be introduced by Sonogashira coupling of the arylbromide **7** with the monoprotected bisacetylene dimer **8**.[38] In preceding optimization efforts, the remaining bromo group of a similar test compound scarcely reacted with **8** under previously used Sonogashira conditions (50 °C). The conversion rate improved when the bromide coupling conditions were applied following Herrmann et al. ([$Pd_2(dba)_3$], P(*t*-Bu)$_3$, NEt_3, 80 °C,

(38) Mössinger, D.; Jester, S.-S.; Sigmund, E.; Müller, U.; Höger, S. *Macromolecules* **2009**, *42*, 7974–7978.
(39) The time-consuming three-step extension of the spokes in the previous synthesis toward prototype **2** strongly demanded optimization.
(40) Lopez, S.; Fernandez-Trillo, F.; Midon, P.; Castedo, L.; Saa, C. *J. Org. Chem.* **2005**, *70*, 6346–6352.
(41) Gaefke, G.; Höger, S. *Synthesis* **2008**, *2008*, 2155–2157.
(42) Höger, S.; Bonrad, K. *J. Org. Chem.* **2000**, *65*, 2243–2245.
(43) In the previous synthesis, the tedious product separation from side products and starting material with similar polarity further decreased the yields of most steps.
(44) Balaban, A. T.; Balaban, T. S. In *Science of Synthesis; Houben-Weyl Methods of Molecular Transformations*; Thomas, E. J., Ed.; Thieme: Stuttgart, 2003; Vol. 14, pp 11−200.
(45) Zimmermann, T.; Fischer, G. W. *J. Prakt. Chem.* **1987**, *329*, 975–984.
(46) Höger, S.; Rosselli, S.; Ramminger, A.-D.; Enkelmann, V. *Org. Lett.* **2002**, *4*, 4269–4272.
(47) The 2-fold Suzuki reaction in the previous synthesis demanded more laborious conditions as well as a more difficult chromatographic purification and afforded lower yields.

33% yield).[48] The best results for the test compound were obtained by applying an *in situ* variant of Plenio's ready-made catalyst mixture (69% yield),[49] that is, with free phosphine instead of $(t\text{-Bu})_3PH^+BF_4^-$ and without $(i\text{-Pr})_2NH_2^+Br^-$ as a catalyst matrix salt. These optimized conditions could be transferred one-to-one to the current synthesis. $Na_2[PdCl_4]$, CuI, and $(t\text{-Bu})_3P$ smoothly catalyzed the coupling of **7** and **8** in $(i\text{-Pr})_2NH$ at 80 °C and gave yields around 90%. Treatment of **9** with potassium carbonate selectively cleaved the CPDMS protective group and produced the final spoke/rim module **10** in close to quantitative yields. In the critical 6-fold Sonogashira coupling of the hub module **4** and the spoke/rim module **10** toward **11** (Scheme 3), we slightly changed the well-established conditions from the previous synthesis.[23] Although still 10 mol % of palladium(II) catalyst was employed per reactive site (0.6 equiv in total), we further increased the overall concentration of the reaction partners to approximately 0.15 M (in the case of **10**), omitted THF as solvent, raised the reaction temperature to 80 °C, and stopped the reaction after one night. **11** could be completely separated from small amounts of the 4- and 5-fold coupling products by column chromatography and was obtained in yields from 73% to 78%.[50] If the reaction was conducted with significantly lower catalyst load (0.1 equiv in total), **11a** could still be isolated in 57% yield, but the separation from incomplete coupling side products became more tedious.[51] Initially, the desilylation of **11** toward **12** also caused some unexpected trouble. To completely remove all CPDMS groups, we added a 1.0 M solution of TBAF in THF at room temperature and stirred overnight. However, this harsh treatment produced **12** along with oligomeric impurities, which could be removed by preparative gel permeation chromatography (GPC) only. When a more dilute solution of TBAF (0.25 M in THF) was added at 0 °C and the reaction was stopped after 3 h, pure **12** could be obtained, even though in suboptimal yields (86−92%).

According to the covalent-template principle, **12** bears 12 adjacent terminal acetylenes and supports its 6-fold intramolecular oxidative coupling. Intuitively, we applied the previously reported copper(I)-catalyzed cyclization conditions on **12a**.[23] A solution of the crude product was filtered over a silica gel column to remove the copper catalyst. GPC analysis revealed a mixture of 85% of the desired spoke wheel **3a** (11 900 g mol^{-1}) and 15% of the dimer and higher oligomers (Figure 1a). However, purification by preparative recycling GPC separation and precipitation with methanol afforded only small amounts of the pure spoked wheel (yields around 20%). Apart from substance losses during the purification procedure, this poor recovery rate must be due to partial polymerization of **12a** during the cyclization reaction and retention of the polymer and higher oligomers by the silica gel column. However, under pseudo high-dilution conditions, intermolecular side reactions can only occur if the intramolecular reaction proceeds slowly. We assumed that pyridine is not basic enough to deprotonate the terminal acetylenes of electron-rich **12a**. Consequently, the overall yield and the cycle/oligomer ratio could be improved in consecutive reactions by the addition of 1,8-diazabicyclo[5.4.0]undec-7-ene (DBU) as strong auxiliary base (Figure 1b) and even more when the latter reaction was performed at 50 °C (Figure 1c). Under optimized reaction conditions, subsequent column chromatography, and precipitation with methanol, **3a** was obtained in 75% yield without detectable oligomer contamination and did not require further purification steps such as preparative GPC.

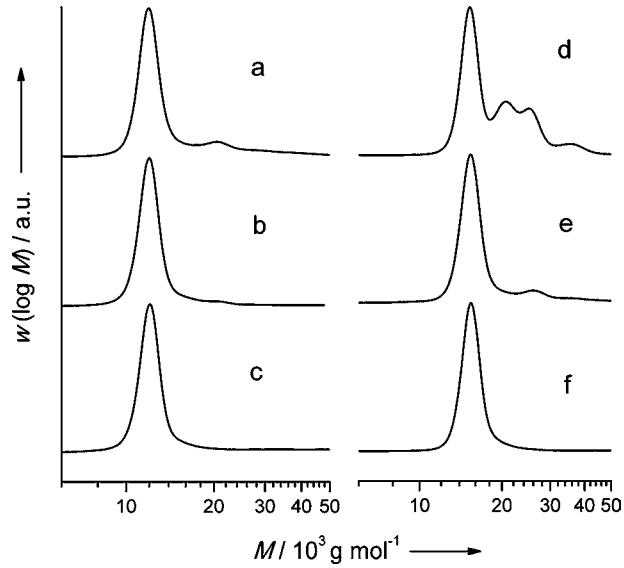

Figure 1. GPC analyses (in THF vs PS) of the crude cyclization products of **3a** (a−c) and **3b** (d,e). Conditions were (a) CuCl, $CuCl_2$, pyridine, room temperature, 4 d; (b) CuCl, $CuCl_2$, DBU (2%, v/v), pyridine, room temperature, 4 d; (c) CuCl, $CuCl_2$, DBU (2%, v/v), pyridine, 50 °C, 4 d; (d) CuCl, $CuCl_2$, DBU (2%, v/v), pyridine, 50 °C, 4 d; (e) $[PdCl_2(PPh_3)_2]$, CuI, I_2, THF, $HN(i\text{-Pr})_2$, 50 °C, 3 d; (f) pure **3b** after recycling GPC purification of the above crude products. See the Supporting Information for GPC analyses of pure **3a**, **12a**, and **12b**.

Oddly, the optimized conditions for the cyclization of **12a** could not be transferred to the hexadecyl precursor **12b**, but produced an oligomeric mixture that contained less than 55% of **3b** (16 200 g mol^{-1}, Figure 1d). As a consequence, we completely discarded our established set of reagents and switched to palladium-catalyzed cyclizations in diisopropylamine/THF with iodine as oxidant.[52] This approach brought considerable improvements toward a wheel/oligomer ratio of about 17:3 (Figure 1e) when a catalyst system consisting of $[PdCl_2(PPh_3)_2]$ and CuI was applied.[53] Still, after column chromatography, the product was not obtained as pure as **3a** and thus required recycling GPC separation. Subsequent precipitation afforded pure **3b** in 64% yield (Figure 1f; for details, see the Supporting Information). Despite the recycling GPC separation during the last step, a 50 mg amount of substance was easily obtained in a simple run of the complete synthesis over seven steps (see TOC graphic). Still, all C−C coupling reactions took place in miniature flasks (1−5 mL) aside from the cyclization step, which was performed under pseudo high-dilution conditions (20 mL reaction volume).

As for spoked wheel **2**, the target compounds appeared as slightly yellow solids, which can be easily handled in solution and stored under air exposure. The large number of alkyl chains afforded a better solubility than for **2**. **3a**'s hexyl chains lead to

(48) Böhm, V. P. W.; Herrmann, W. A. *Eur. J. Org. Chem.* **2000**, 3679–3681.
(49) Köllhofer, A.; Plenio, H. *Adv. Synth. Catal.* **2005**, *347*, 1295–1300.
(50) Note that 78% in a 6-fold reaction corresponds to 96% in each of the six coupling reactions per molecule.
(51) Those conditions were not applied for the synthesis of **11b**.
(52) Marsden, J. A.; Miller, J. J.; Haley, M. M. *Angew. Chem., Int. Ed.* **2004**, *43*, 1694–1697.
(53) $[PdCl_2(dppe)]$ was only tried once. The HT ^1H NMR spectrum of the GPC-separated main fraction showed a minor singlet peak at $\delta = 3.34$ ppm, possibly a hint at an incomplete terminal acetylene conversion during the cyclization reaction.

Table 1. GPC Peaks ($M_{p,i}$) and Molar Masses (M_{abs}) of **10**, **12**, and **3**

compound	M_{abs}/g mol^{-1}	M_p^{GPC} (vs PS)/g mol^{-1}	$M_{vs\ PS}^{GPC}/M_{abs}$
10a	1971.13	2800	1.42
12a	10 173.19	12 900	1.27
3a	10 161.09	11 900	1.17
10b	3093.26	4500	1.45
12b	16 905.95	16 200	0.96
3b	16 893.85	15 400	0.91

increased solubility in chloroform (>50 mg mL^{-1}), but are obviously not that effective in THF, toluene, and dichloromethane. By contrast, the hexadecyl-substituted wheel (**3b**) showed enhanced solubility in all solvents discussed above and could even be dissolved in cyclohexane as monomeric species (see DLS investigations). **3a** does not melt below 250 °C and decomposes above that temperature. Because the noncyclic precursor **12b** was obtained as a resin even after precipitation with methanol, we anticipated finding a low melting point for **3b**. Instead, the material does not undergo any change apart from a solid/liquid-crystalline transition at 225 °C. Unfortunately, decomposition already occurred to some extent in the liquid crystalline state, so that neither could a transition into an isotropic melt be observed, nor could the LC phase be analyzed in detail (see the Supporting Information for differential scanning calorimetry (DSC) thermograms and polarization microscopy).

GPC Analysis

GPC analysis does not only reveal product mixtures but can be a monitor for successful cyclization. Although the actual mass difference is only 12 mass units (see Figure 3), PS-calibrated GPC interprets this difference as 1.0×10^3 g mol^{-1} (**12a** > **3a**, R = C_6H_{13}) and 0.8×10^3 g mol^{-1} (**12b** > **3b**, R = $C_{16}H_{33}$), respectively (for elugrams of **12a** and **12b**, see the Supporting Information). Table 1 summarizes all GPC data for the compounds **3**, **10**, and **12** and points out two apparent tendencies for both spoked wheels **3a** and **3b** and their respective precursors. (1) The more the molecules resemble flat rigid disks, the smaller is the molecular weight overestimation by GPC (**10** > **12** > **3**). (2) With increasing length (and number) of the alkyl chains attached to the rigid backbone, the relative overestimation of the molecular weight by GPC decreases (**12a** > **12b**, **3a** > **3b**). Because of the branched structure of **10**, the overestimation factor (1.4) is considerably lower than for linear rigid systems.[38,54] This trend becomes even more pronounced after the 6-fold coupling of **10** to the hub **4**. Cyclization reduces the hydrodynamic radius because spoke/rim moieties of **12** are forced into a coplanar conformation and lose their rotational degrees of freedom around the spoke axes. As a result, the loss of 12 acetylene protons is strongly overestimated by GPC. Because the hydrodynamic radii of the spoked wheel and the open precursors are, roughly speaking, determined by their diameter, the higher molecular weight of **3b** as compared to **3a** (and also **12b** vs **12a**) is not completely reflected by a similar higher molecular weight determination by GPC. An error cancelation finally leads to the situation that the GPC analysis of **12b** and **3b** with PS calibration reflects the correct molecular weight within an error of 10%.

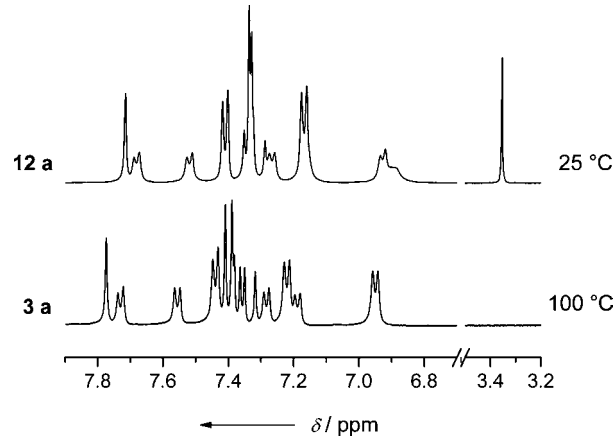

Figure 2. ^{1}H NMR spectra (500 MHz, $C_2D_2Cl_4$): the aromatic region of the open precursor (**12a**, 25 °C, top) exhibits some signals, which are masked in the better resolved high-temperature spectrum of the spoked wheel (**3a**, 100 °C, bottom) and vice versa. The absence of terminal acetylene signals (around δ = 3.35 ppm) in the spectrum of **3a** is an indication of complete cyclization. For full spectra of **3a**, **3b**, **12a**, and **12b**, see the Supporting Information.

High-Temperature NMR Investigations

Typically, room-temperature (RT) NMR spectra of **3** show broadened signals, as the phenylene units directly attached to the hub and the corner pieces are expected to have considerable rotational barriers.[23] As shown in Figure 2, the aromatic region of the wheel spectrum (**3a**, bottom) obtained from high-temperature (HT) ^{1}H NMR measurements at 100 °C in deuterated 1,1,2,2-tetrachloroethane is comparable to the RT spectra of the precursor (**12a**) (top, for spectra of **3b** and **12b**, see the Supporting Information).[55]Apart from significant temperature shifts, which reveal a merged signal group in the spectrum of **3a** (δ = 6.95 ppm), the aromatic regions of the precursor and the wheel are similar. The small number of signal groups despite 180 aromatic hydrogen atoms per molecule accounts for the high symmetry of both **3** and **12**. The small cutout of the alkyl region (Figure 2, right) shows terminal acetylene signals at δ = 3.35 ppm in the spectrum of **12a** (top) and the absent signal as one proof of cyclization in the spectrum of **3a** (bottom). Substance quantities were sufficient for HT ^{13}C NMR measurements of **3a** and **3b** in deuterated tetrachloroethane. Considering the size of the molecules (**3a**, $C_{774}H_{858}$; **3b**, $C_{1254}H_{1818}$), the ^{13}C spectra are surprisingly concise, which is again a consequence of the high symmetry of the spoked wheel scaffold (see the Supporting Information).

MALDI MS Measurements

For the prototype wheel **2**, we drew on MALDI-TOF MS as a powerful method to prove complete cyclization and the molecular uniformity of the sample.[18,23] Accordingly, for each pair of precursor/spoked wheel (**3** and **12**), a mass difference of approximately 12 mass units could be resolved, which corresponds to the loss of 12 acetylene protons in the course of cyclization (Figure 3). Alkyl fragmentation occurs particularly in the spectra of **12a** (left, gray curve) and **12b** (right, gray curve), whereas **3a** (left, black curve) and **3b** (right, black curve) seemed to be more resistant to the conditions of the measurement and, in addition, hardly formed any matrix adducts (matrix material: dithranol). The loss of alkyl side chains and the

(54) Xu, Z.; Kahr, M.; Walker, K. L.; Wilkins, C. L.; Moore, J. S. *J. Am. Chem. Soc.* **1994**, *116*, 4537–4550.
(55) A similar behavior is also observed for the prototype spoked wheel **2**.

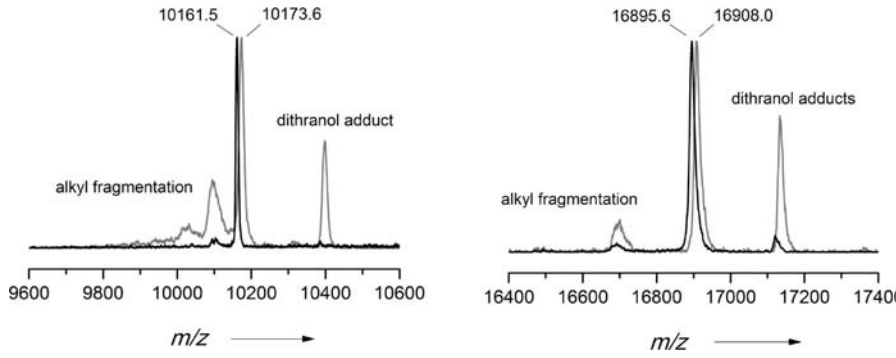

Figure 3. MALDI-MS spectra of the spoked wheels (black) and the respective noncyclic precursors (gray). Both for **3a**/**12a** (left) and for **3b**/**12b** (right), a difference of approximately 12 *m*/*z* was found. The fragmentation peaks can most probably be attributed to the loss of C_5H_{10} and $C_{15}H_{30}$ units due to McLafferty rearrangement. Matrix material: dithranol (226.23 g mol^{-1}).

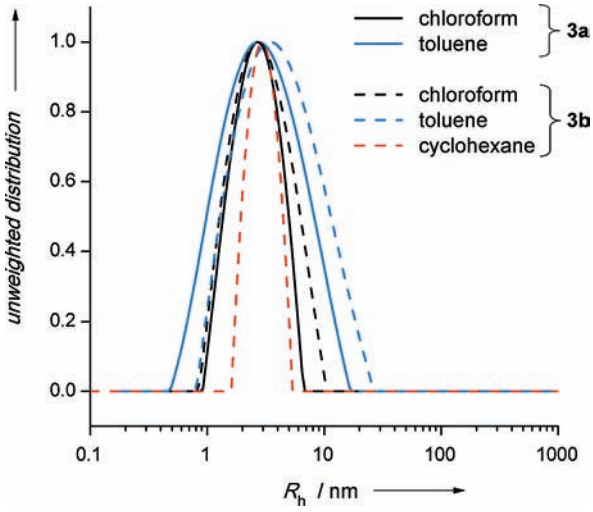

Figure 4. Hydrodynamic radius (R_h) distributions obtained from dynamic light scattering (DLS) experiments on samples of **3a** (continuous line; 1.0 $\times$ 10^{-4} mol L^{-1}) and **3b** (dashed line; 0.6 $\times$ 10^{-4} mol L^{-1}) in chloroform (black), toluene (blue), and cyclohexane (red). For all solvents investigated, only monomer-sized diffusing particles can be observed.

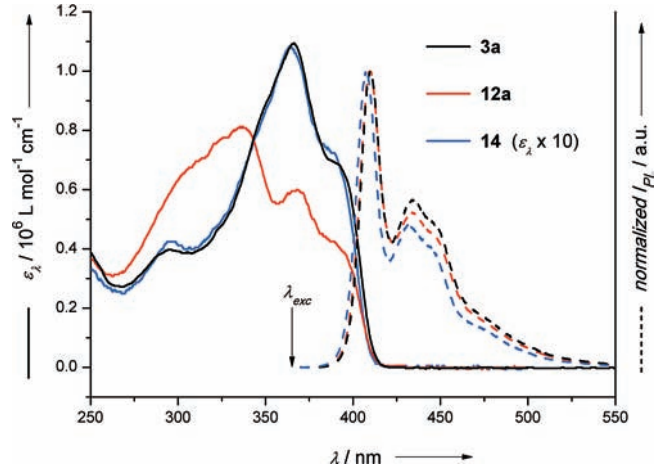

Figure 5. Quantitative UV−vis absorption spectra (continuous lines) and normalized emission spectra (dashed lines, λ_{exc} = 365 nm) of the spoked wheel (**3a**, black), the noncyclic precursor (**12a**, red), and the linear model rod (**14**, blue, Scheme 4) in $CHCl_3$. Note that **14** constitutes a suitable model chromophore both for the absorption and for the emission of the spoked wheel. See Table 2 for the molar absorption coefficients and fluorescence quantum yields.

formation of sample-matrix clusters are known phenomena, which particularly occur at medium to high laser powers.[56]

Aggregation Studies (DLS)

In preparation for the photophysical studies, we aimed to ensure that the spoked wheels **3a** and **3b** do not form aggregates (e.g., columnar stacks) in solution. On this account, we performed dynamic light scattering (DLS) investigations of dilute solutions of **3a** (continuous line; 1.0 $\times$ 10^{-4} mol L^{-1}) and **3b** (dashed line; 0.6 $\times$ 10^{-4} mol L^{-1}) in chloroform and toluene at 20 °C (Figure 4). The chloroform solutions (black curves) of both spoked wheels contained only one scattering (and diffusing) species with a hydrodynamic radius distribution from roughly 1 to 10 nm and maxima at 2.7 and 3.5 nm, respectively. In contrast to the hexyl-decorated **3a**, the hexadecyl derivative **3b** is even well soluble in cyclohexane. Here again, as it holds for the chlorinated and the aromatic solvent, the only scattering species detected by DLS was nonaggregated **3b** (Figure 4, dashed red curve). As intended, the solubilizing groups orthogonal to the plane of the wheel are sufficient to prevent stacking and aggregation in solution. Hence, in dilute solutions we can be sure to determine the optical properties of individual molecules without any (intermolecular) cooperative effects.

Optical Properties

Absorption measurements of both spoked wheels in chloroform reveal structured absorption bands stretching from 270 to about 410 nm with maxima at 366 nm (**3a**, Figure 5, black curve; **3b**, see the Supporting Information). As expected, we found nearly identical absorption and emission spectra for the spoked wheels **3a** and **3b** as well as for the noncyclic precursors **12a** and **12b**, respectively (see Figure 5 and the Supporting Information). Obviously, the alkyl chain length does not influence the rigid backbone conformation in such a manner that the relative absorption of different chromophores within the molecule changes. As already illustrated for the prototype,[23] **3a** (Figure 5, black curve) and **3b** can also be distinguished from their noncyclic precursors **12a** (red curve) and **12b** by their absorption spectra. For **2** and its precursor **1**, we explained these findings by the presence of different absorbing chromophores in **1** and **2**, but identical fluorophores.[23] The new, more symmetrical wheels **3a** and **3b** consist of identical chromophores both in the spokes and in the rim segments and therefore encourage a closer look at the optical properties.

(56) Höger, S.; Spickermann, J.; Morrison, D. L.; Dziezok, P.; Räder, H. J. *Macromolecules* **1997**, *30*, 3110–3111.

Scheme 4. Local Assignment and Syntheses of the Linear Model Chromophores **14** and **16**

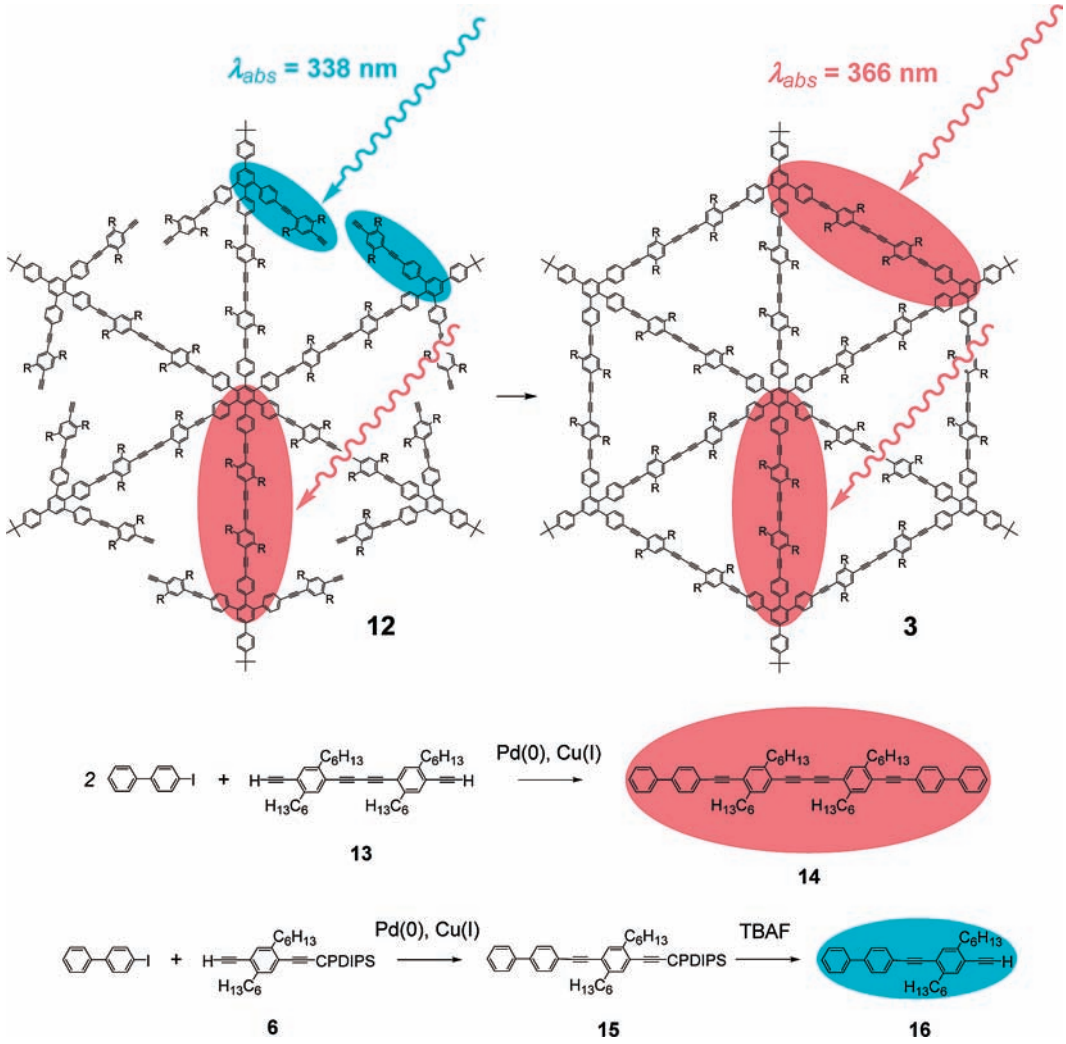

Table 2. Molar Absorption Coefficients (in $CHCl_3$) and Fluorescence Quantum Yields (in THF) of the Compounds Discussed (±5% Accuracy)

compound	λ_{max}/nm	ε_λ/L mol^{-1} cm^{-1}	Φ_{PL} (in THF)
3a	366	1.06×10^6	0.51
12a	338	0.81×10^6	0.58
	366	0.60×10^6	
14	365	0.11×10^6	0.56
16	323	0.44×10^5	

Again, upon excitation (λ_{exc} = 365 nm) both the spoked wheels and their precursors exhibit almost congruent emission spectra (Figure 5, right) with maxima at 409 nm and stretched vibronic progression features. Because of the constrained geometry of the molecules, we find small Stokes shifts of about 43 nm (23 250 cm^{-1}) resulting in a spectral overlap of absorption and emission. Molecular models indicate that the six phenylene units surrounding the central benzene hub are considerably twisted out of the molecular plane, leading to a "turbine-like" conformation of the spokes. Hence, the conjugation between two opposite spokes must be interrupted. If we further presume a perturbation of conjugation by the *meta*-linkage at the corners,[57] the wheel's most extended chromophore is formed by either one linear rim segment or a single spoke. Because of the high symmetry of **3a** and **3b**, the rim segments and spokes consist of nearly identical linear chromophores and can be modeled by the same model compound **14** (Scheme 4).

As a matter of fact, **14**'s absorption and emission spectra (Figure 5, blue curves) are comparable to those of the spoked wheel (black curve), which implies that absorption and emission of **3a** predominantly occur from the linear segments (6 spokes + 6 rim segments). The respective absorption coefficients support this finding (Table 2). The molar absorption coefficient of **3a** at 366 nm is about 10 times as large as that of the model chromophore **14** (also Figure 5). Hence, spoked wheels **3a** and **3b** can be regarded as covalently bound ensembles of linear chromophores of various orientations.

Apart from identical emission spectra,[58] the characteristic absorption band of **14** (λ_{max} = 365 nm and shoulder around 390 nm) is also present in the spectrum of the noncyclic precursor **12a** (Figure 5, red curve). Because the rim segments are still "cut in half", this absorption must originate from the spokes. However, **12**'s main band (λ_{max} = 338 nm) must be contributed by less conjugated, but more numerous chromophores and can hence be assigned to the half-rim segments (represented by **16**). This hypothesis can be verified by taking

(57) Boldi, A. M.; Diederich, F. *Angew. Chem., Int. Ed. Engl.* **1994**, *33*, 468–471.

(58) **12**'s emission exclusively emanates from the spokes, even if excited at 325 nm.

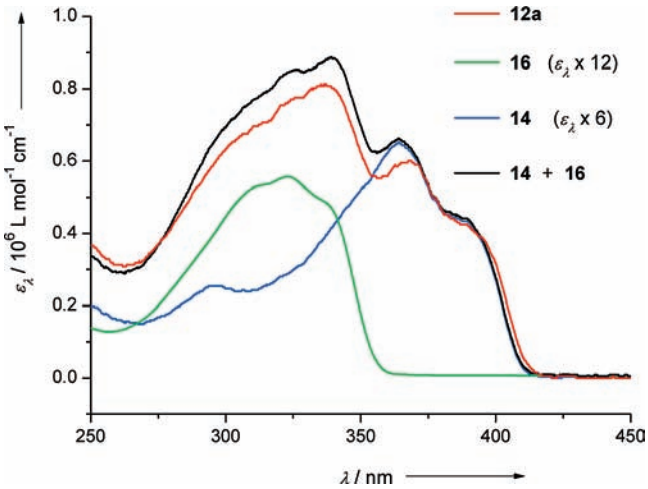

Figure 6. Comparison of the noncyclic precursor's absorption spectrum (**12a**, red) and the sum spectrum (black) composed of the model compounds **14** (blue, 6-fold contribution) and **16** (green, 12-fold contribution). Apart from small differences in extinction, the spectrum of **12a** can be reproduced by a weighted combination of the model compound spectra (**14** and **16**). See Table 2 for the molar absorption coefficients.

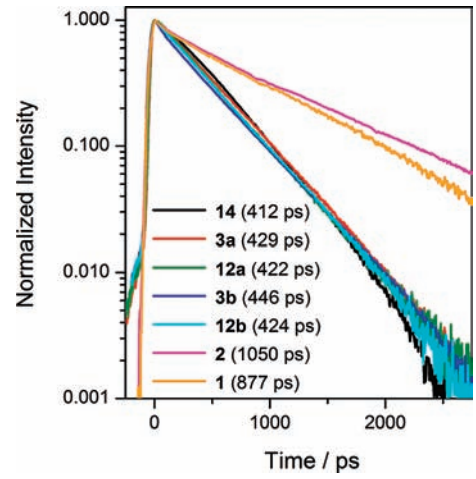

Figure 7. Fluorescence intensity decay curves for the model compound **14**, wheels **3a**, **3b**, and **2**, and their corresponding noncyclic precursors **12a**, **12b**, and **1**, respectively. The fluorescence lifetime for each sample is given in parentheses. The lifetime depends solely on the length of the emissive chromophore.

the absorption coefficients into account (Table 2). **12a**'s absorption spectrum can be approximately composed of the absorption spectra of the model compounds, because **12a** should contain six spoke chromophores **14** and 12 half rim segment chromophores **16**. Figure 6 demonstrates the good agreement of the spectrum obtained by summation of the constituent absorptions with the actual absorption spectrum of **12a**.

The absorption coefficients reveal some further details. As listed in Table 2, the absorption of precursor **12a** is dominated by the half rim segments (main band, $\lambda_{max} = 338$ nm). However, the band originating from the spokes' absorption ($\lambda_{max} = 366$ nm) can be compared to the main bands of the spoked wheel **3a** and the rod model **14**, which appear at similar wavelengths. Remarkably, we find a nearly additive relation between **3a**, **12a**, and **14**. The absorption coefficient of the precursor **12a** (366 nm, 6 chromophores) is almost 6 times as large as that of the model **14** (1 chromophore) and constitutes about 57% of the spoked wheel's absorption coefficient (**3a**, 12 chromophores).

Time-Resolved Optical Investigations and Energy Transfer

To unravel the interaction pathways between chromophores within a wheel, we considered the transient fluorescence dynamics. Fluorescence intensity decay curves of three different molecular wheels (**3a**, **3b**, and **2**) and their broken-rim (noncyclic) precursors (**12a**, **12b**, and **1**, respectively) are shown in Figure 7. All decay traces could be fitted by a single exponential function. Compounds **3a** and **3b** are structurally similar except for the length of the alkyl side chain. **2**, on the other hand, is a smaller molecule, and therefore has a shorter chromophore. We find that the fluorescence lifetimes depend solely on the conjugation length of the emissive chromophore.[59] Because the fluorophore in these molecular wheels is defined by the length of the spoke, its degree of conjugation is not influenced by the integrity of the outer rim. Consequently, the cyclic wheels and the corresponding noncyclic precursors exhibit nearly overlapping decay curves. For sake of comparison, the fluorescence decay curve of the model compound **14** is also presented in Figure 7. Once again, we find that **14** is an accurate representation of the chromophoric segment in **3a**, as it exhibits identical decay kinetics. The alkyl chain lengths do not affect the emission properties of these rigid molecular wheels or their noncyclic counterparts, and consequently the fluorescence lifetimes of the hexyl and hexadecyl analogues are identical. The molecules with shorter conjugated chromophoric segments (**2** and **1**) quite expectedly show a 2.5-fold slower fluorescence decay,[59,60] due to a reduction in oscillator strength arising from fewer electrons participating in conjugation.

Because of a highly regular and well-defined molecular architecture, these multichromophoric wheels also make interesting candidates for the investigation of intramolecular excitation energy transfer mechanisms relevant for light harvesting.[15,61,62] In such systems, one of the fundamental challenges is to understand the strength of interchromophoric interactions.[63,64] Fluorescence depolarization measurements offer a unique way to study the dynamics of the photoexcitation energy transfer between different chromophoric segments within the same molecule.[15,65,66] As the excitation moves from one chromophore to the other, the transition dipole reorients itself, leading to a depolarization of the emission. Experimentally, fluorescence depolarization can be monitored by the change in polarization anisotropy, r, determined by measuring the emission polarization parallel and orthogonal to the excitation polarization [$r = (I_{||} -$

(59) Schindler, F.; Jacob, J.; Grimsdale, A. C.; Scherf, U.; Müllen, K.; Lupton, J. M.; Feldmann, J. *Angew. Chem., Int. Ed.* **2005**, *44*, 1520–1525.

(60) The decrease in fluorescence lifetime with increasing conjugation length is caused by several effects: (1) highly efficient intramolecular energy transfer, (2) reduced vibronic coupling, (3) increased oscillator strength, and (4) singlet state trapping defects.

(61) Ghiggino, K. P.; Reek, J. N. H.; Crossley, M. J.; Bosman, A. W.; Schenning, A. P. H. J.; Meijer, E. W. *J. Phys. Chem. B* **2000**, *104*, 2596–2606.

(62) De Schryver, F. C.; Vosch, T.; Cotlet, M.; Van der Auweraer, M.; Müllen, K.; Hofkens, J. *Acc. Chem. Res.* **2005**, *38*, 514–522.

(63) Varnavski, O. P.; Ostrowski, J. C.; Sukhomlinova, L.; Twieg, R. J.; Bazan, G. C.; Goodson, T. *J. Am. Chem. Soc.* **2002**, *124*, 1736–1743.

(64) Scholes, G. D. *Annu. Rev. Phys. Chem.* **2003**, *54*, 57–87.

(65) Varnavski, O.; Menkir, G.; Goodson, T.; Burn, P. L. *Appl. Phys. Lett.* **2000**, *77*, 1120–1122.

(66) Ruseckas, A.; Wood, P.; Samuel, I. D. W.; Webster, G. R.; Mitchell, W. J.; Burn, P. L.; Sundstrom, V. *Phys. Rev. B: Condens. Matter* **2005**, *72*, 115214.

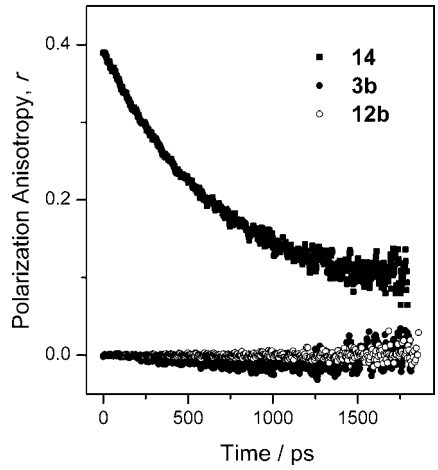

Figure 8. Time-dependent polarization anisotropy of the model linear chromophore **14** (■), wheel **3b** (●), and noncyclic precursor **12b** (○). While the linear chromophore shows gradual depolarization of emission due to molecular tumbling in solution, the wheel and its noncyclic precursor undergo ultrafast depolarization mediated by rapid interchromophoric energy transfer.

$I_\perp)/(I_\parallel + 2I_\perp)]$. For an isotropic arrangement of linear dipoles, the value of r is 0.4.[67] However, in the solution phase, polarization can be lost due to rotational diffusion of the emitting molecule or energy transfer, the two mechanisms having very different time scales. Figure 8 presents the time-dependence of polarization anisotropy of the linear model compound **14**, spoked wheel **3b**, and its noncyclic precursor **12b**. The linear model compound exhibits an initial anisotropy value of 0.39 that decreases steadily due to rotational diffusion. The emission from the bigger molecules, on the other hand, is completely depolarized right at the onset. Clearly, the loss of polarization, which is a consequence of rapid interchromophoric energy transfer, happens on time scales shorter than the resolution of our measurement of about 2 ps. It is interesting to note that the wheel and its noncyclic precursor exhibit an equally rapid depolarization, within the accuracy of our measurements. This suggests that resonant dipole−dipole coupling can occur between different chromophores arranged around a central benzene hub, quite similar to what is observed in certain star-shaped molecules.[63] It is possible that the wheels have an additional energy transfer pathway through the rim. However, the energy transfer around the central hub is so much faster than our resolution limit that it is not possible to distinguish between the cyclic wheel and its noncyclic precursor. It is interesting to note that such a rapid interchromophoric energy transfer in these molecules does not affect their fluorescence quantum efficiencies. The photoluminscence quantum efficiencies for **3a** (wheel), **12a** (open precursor), and **14** (linear model compound) are very similar (0.54 ± 0.04) (Table 2). Ultrafast depolarization in multichromophoric, π-conjugated systems has been associated with a coherent delocalization of the excited state across strongly coupled chromophores.[63,68,69] We, however, believe that these molecular wheels represent a case of weakly coupled chromophores. As discussed above, molecular modeling suggests that in the ground state, the phenylene units of the hexaphenylbenzene hub assume a "turbine-like" geometry, so that the spokes (chromophores) are twisted out of the molecular plane. Consequently, the π-conjugation is limited within an individual spoke. Furthermore, the fact that the model compound **14** and spoked wheel **3a** have identical fluorescence lifetimes suggests that even in the excited state, the extent of conjugation is limited only to individual spokes. The wheels therefore resemble an ensemble of weakly interacting linear chromophores. This is further substantiated by the fact that the molar extinction coefficient, which is also a measure of the electronic oscillator strength, scales almost linearly with the number of chromophores (see Table 2).[70]

Scanning Tunneling Microscopy

Deposition of **3a** and **3b** from 1-phenyloctane onto highly ordered pyrolytic graphite (HOPG) leads to the appearance of close-packed hexagon-shaped bright objects, as revealed by scanning tunneling microscopy (STM) at the solid/liquid interface (Figures 9 and 10). The bright protrusions in the STM images are attributed to the unsaturated backbones of the molecules, whereas the dark areas inside the hexagons are empty or occupied by disordered solvent molecules or alkyl side chains.[71] By comparison of the diameter of the hexagons with a molecular model (vide infra), it can be concluded that the hexagons correspond to individual molecules. High-resolution images (Figures 9b and 10b) reveal the internal structure of the molecules. The voids inside the molecules do not provide enough space for adsorption of all side chains. We expect that some or all side chains of the spokes and inner sides of the rims are solvated as has been previously reported for other alkylated molecules at solid/liquid interfaces.[72]

Despite the large number of hexadecyl chains orthogonal to the plane of the spoked wheel, the 2D ordering of **3b** at the solid−liquid interface is surprisingly good (Figure 10). The periodicity of **3b** molecules (8.7 nm) is markedly greater as compared to the periodicity of **3a** molecules (7.0 nm), which is attributed to the difference in the length of the alkyl chains. As deduced from small-scale images such as Figure 10b, parallel sides of adjacent molecules are linked by four interdigitated alkyl chains. Based on the available experimental data, models reflecting the molecular packing were built. Upon close inspection of these models (Figures 9c and 10c) and the experimental data, it is obvious that the self-assembled monolayers formed by **3a** and **3b** are chiral. The spokes of the molecules do not point right to the center between the two nearest molecules. A negative or positive angle between the orientation of the spokes and the center between the two next-nearest neighbor molecules determines the chirality of the domain. Consequently, domains with opposite chirality were observed (not shown).[23]

Atomic Force Microscopy

To probe the self-assembling properties of these molecules beyond monolayer formation, atomic force microscopy (AFM) studies were carried out. Figure 11 shows the typical assembly formed by **3a** on a graphite surface upon dropcasting a toluene

(67) Lacowicz, J. R. *Principles of Fluorescence Spectropscopy*; Springer: New York, 1999.
(68) Ranasinghe, M. I.; Wang, Y.; Goodson, T. *J. Am. Chem. Soc.* **2003**, *125*, 5258–5259.
(69) Lupton, J. M.; Samuel, I. D. W.; Burn, P. L.; Mukamel, S. *J. Phys. Chem. B* **2002**, *106*, 7647–7653.
(70) Kopelman, R.; Shortreed, M.; Shi, Z.-Y.; Tan, W.; Xu, Z.; Moore, J. S.; Bar-Haim, A.; Klafter, J. *Phys. Rev. Lett.* **1997**, *78*, 1239.
(71) In the constant current mode, the dark-white contrast refers to the STM tip height: the brighter it is, the larger is the tip−substrate separation.
(72) Tahara, K.; Furukawa, S.; Uji-i, H.; Uchino, T.; Ichikawa, T.; Zhang, J.; Mamdouh, W.; Sonoda, M.; De Schryver, F. C.; De Feyter, S.; Tobe, Y. *J. Am. Chem. Soc.* **2006**, *128*, 16613–16625.

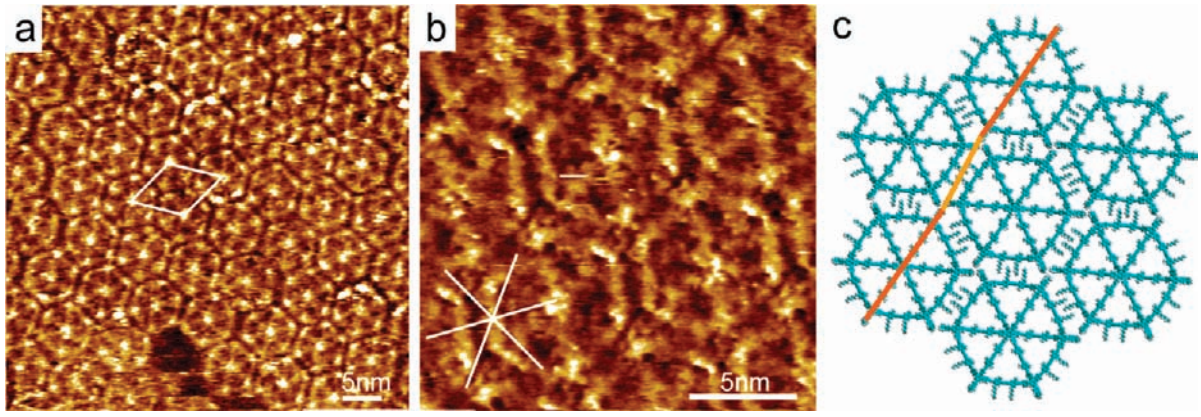

Figure 9. STM images and tentative molecular packing model of **3a** self-assembled at the 1-phenyloctane/graphite interface. (a) 46.9 × 46.9 nm^2, I_{set} = 19 pA, V_{bias} = −0.915 V. The *p*6 symmetry unit cell with parameter a = 7.0 ± 0.4 nm is indicated in white. (b) High-resolution STM image 18.6 × 18.6 nm^2, I_{set} = 19 pA, V_{bias} = −1.154 V. The white lines indicate orientations of the main crystallographic directions of the underlying graphite surface. (c) Schematic representation of the tentative packing model. Red bars highlight the orientation of equivalent spokes in different molecules. The angle between the orange and the red bars demonstrates the chirality induced by lateral offset in the packing. Side chains other than peripheral hexyl groups have been omitted for clarity.

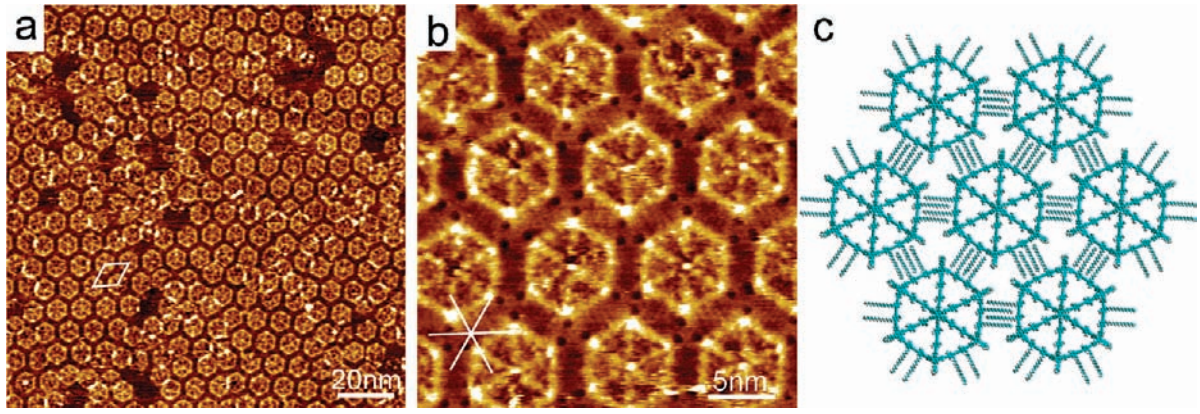

Figure 10. STM images and tentative molecular packing model of **3b** self-assembled at the 1-phenyloctane/graphite interface. (a) 116 × 116 nm^2, I_{set} = 30 pA, V_{bias} = −0.918 V. The *p*6 symmetry unit cell with parameter a = 8.7 ± 0.4 nm is indicated in white. (b) High-resolution STM image 27.7 × 27.7 nm^2, I_{set} = 30 pA, V_{bias} = −0.913 V. White lines indicate orientations of the main crystallographic directions of the underlying graphite surface. (c) Schematic representation of the tentative packing model. Side chains other than peripheral hexadecyl groups have been omitted for clarity.

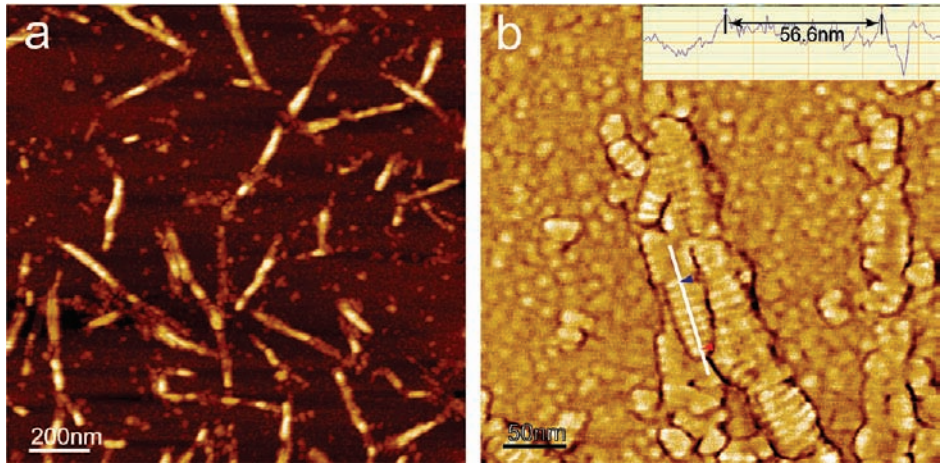

Figure 11. Large-scale height (a) and high-resolution phase image (b) of the self-assembling structure of **3a** deposited from toluene on graphite. Lamellae-like features could be clearly seen in the high-resolution phase image, and their width was estimated at about 8 nm. The section profile along the white line is shown in the inset.

solution. "Fiber"-like features 30 nm in width and 10−12 nm in height were observed. These fibers can extend to hundreds of nanometers, but are not always straight. High-resolution phase images reveal that these fibers are composed of lamellae features oriented perpendicular to the fiber axis. The width of the lamellae was measured to be about 8 nm, roughly consistent with the diameter of the spoked wheel. These images also indicate that these so-called fibers are actually multilayers, with

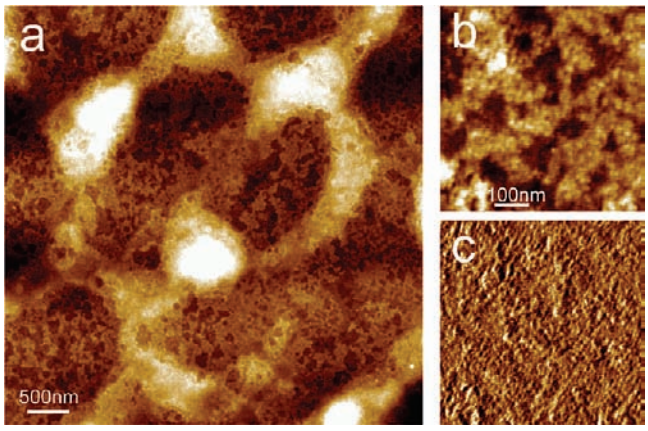

Figure 12. Large-scale (a) and high-resolution (b) height image of **3b** self-assembled from toluene on graphite. (c) Corresponding phase image of image (b).

each layer measuring around 6 nm in height. Considering all of this evidence, we conclude that the lamellae-like features in the fibers correspond to columns of stacked wheel molecules oriented nearly perpendicular to the surface. Besides the fibers, some amorphous features with much lower height were also observed.

For wheel compound **3b**, the AFM observations reveal different characteristics. Instead of fibers, **3b** forms layer-like structures on the graphite surface (Figure 12). On the large scale, this structure looks quite similar to that previously reported for the prototype **2**.[23] The thickness of the layers, about 0.6 nm, also corresponds well with that measured for **2**. However, high-resolution images (Figure 12b) reveal no clear ordering in the layer, which indicates that, except for the monolayer in direct contact with the graphite surface, the long-chain spoked wheels (**3b**) align randomly in the layer with their molecular plane parallel to the surface.

When mica is used as substrate, both **3a** and **3b** show significantly different assembling characteristics as compared to those observed on graphite, as summarized in Figures 13 and 14. In this case, **3a** forms layered assemblies of different height. The thicker layer measured 6.7 nm in height and corresponds well with the diameter of the molecules, while the thinner lower layer measures only 2.5 nm in height. Close inspection reveals that the length of typical stacks of **3a** is limited to around 30 nm. The corresponding phase image reveals no significant ordering in the thinner layer, which indicates that the molecules in this layer are arranged randomly.

Figure 14 shows the self-assembled structure of **3b** on mica: layered structures with different heights are revealed. The thinner layer appears very flat (height of about 0.6 nm), which corresponds to a monolayer of molecules lying with their molecular plane parallel to the surface. The rougher brighter part measures 2.5 nm in height, similar to the amorphous layer of **3a**. Interestingly, the corresponding phase image shows stripe-like features in the thinner layers. The orientation of these stripes is indicated by the green lines in Figure 14b. In high-resolution phase images, the ordering in the flat thin layer could be revealed more clearly as shown in Figure 14d. To our surprise, the fast Fourier transformation (FFT) of the phase image reveals a hexagonal packing, and the repeating period is approximately 5.0 nm, only around one-half of the intermolecular distance observed by STM on graphite (8.7 nm). Considering the diameter of the wheel (only the rigid backbone) is around 6.4 nm (apex-to-apex distance), the repeating period observed here is too small even if we assume that the alkyl chains do not adsorb on the surface. One possibility is that not only the hub but also the *tert*-butyl groups contribute to the phase contrast. If so, the repeating period equals $1/\sqrt{3}$ of the intermolecular distance, which is expected to be 5.02 nm, and is in very good agreement with our observation. This indicates that **3b** forms exactly the same packing on mica as on graphite, sketched in Figure 15, which is quite surprising considering the significant difference in properties of both substrates.

Conclusions

On the basis of the covalent-template approach, a rational modular synthesis toward molecularly defined, rigid, highly symmetrical 2D oligomers has been developed. Two 8 nm-sized hydrocarbon spoked wheel structures, decorated with 48 alkyl side chains of different length, were synthesized in very good yields from simple prefabricated building blocks. Both compounds could be efficiently produced in 50 mg quantities in a single run over seven steps. Because of the high molecular symmetry, the nanoscale materials could be fully characterized despite their size and molecular weights around 10 and 17 kDa, respectively. MALDI-MS investigations as well as concise high-temperature ^{1}H and ^{13}C NMR spectra clearly prove the regular cyclic structure. GPC measurements and comparison with linear rigid compounds reveal an error-canceling effect of the molecular shape and side chain length on the molecular weight overestimation. While the hexyl substituents provide sufficient solubility in THF, toluene, and chlorinated solvents, the hexadecyl-decorated wheel is even soluble in cyclohexane. DLS investigations of dilute solutions of both compounds illustrate that the solubilizing groups attached orthogonal to the molecular plane are sufficient to prevent stacking and aggregation in the solvents that we investigated. Hence, in dilute solutions, we can be sure to determine the optical properties of individual molecules without any cooperative effects.

Detailed UV−vis absorption and emission investigations and comparisons with model chromophores give information about the location and number of isolated linear chromophores within the spoked wheels and their noncyclic precursors. Analogous to linear oligomers and polymers, the fluorescence lifetimes of the spoked wheels merely depend on the length of the longest conjugated chromophore. Fluorescence depolarization measurements reveal an ultrafast (<2 ps) decay of the polarization anisotropy *r*, which is evidence of an intramolecular resonance energy transfer between all linear chromophores located in the spokes and the rim. Therefore, the spoked wheels can be regarded as an ensemble of weakly interacting (identical) linear chromophores, posing an intriguing 2D model system to study molecular light-harvesting phenomena.

STM investigations illustrate that both wheels form periodic 2D monolayers at the solid/liquid interface. Remarkably, the periodicity is efficiently controlled by the length of interdigitating peripheral side chains, while the side chains (orthogonal to the wheel's plane) do apparently not perturb the adsorption. This tight molecular packing results in periodicities of 7.0 nm ($R = C_6H_{13}$) and 8.7 nm ($R = C_{16}H_{33}$), respectively. A comparison with packing models illustrates the layers' *p*6 symmetry. Moreover, the offset caused by the chain interdigitation leads to domains of opposite chirality. AFM studies reveal a very different assembly behavior of the two compounds, on both graphite and mica. The hexyl-decorated wheel shows a stronger tendency to form stacks resulting in columnar superstructures, whereas, most probably because of steric interactions,

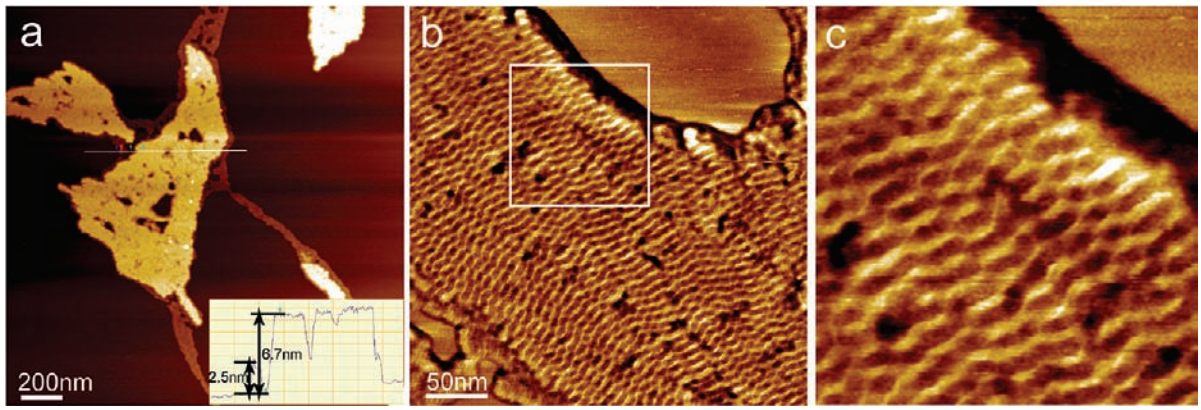

Figure 13. (a) Large-scale height image of **3a** self-assembled on mica surface. Two kinds of layered structures were observed with heights of 2.5 and 6.7 nm, respectively. The high-resolution phase image (b) clearly shows the inner structure of the thicker layer. (c) An enlargement of the area marked by the rectangle in (b) (image size 120 × 120 nm^2).

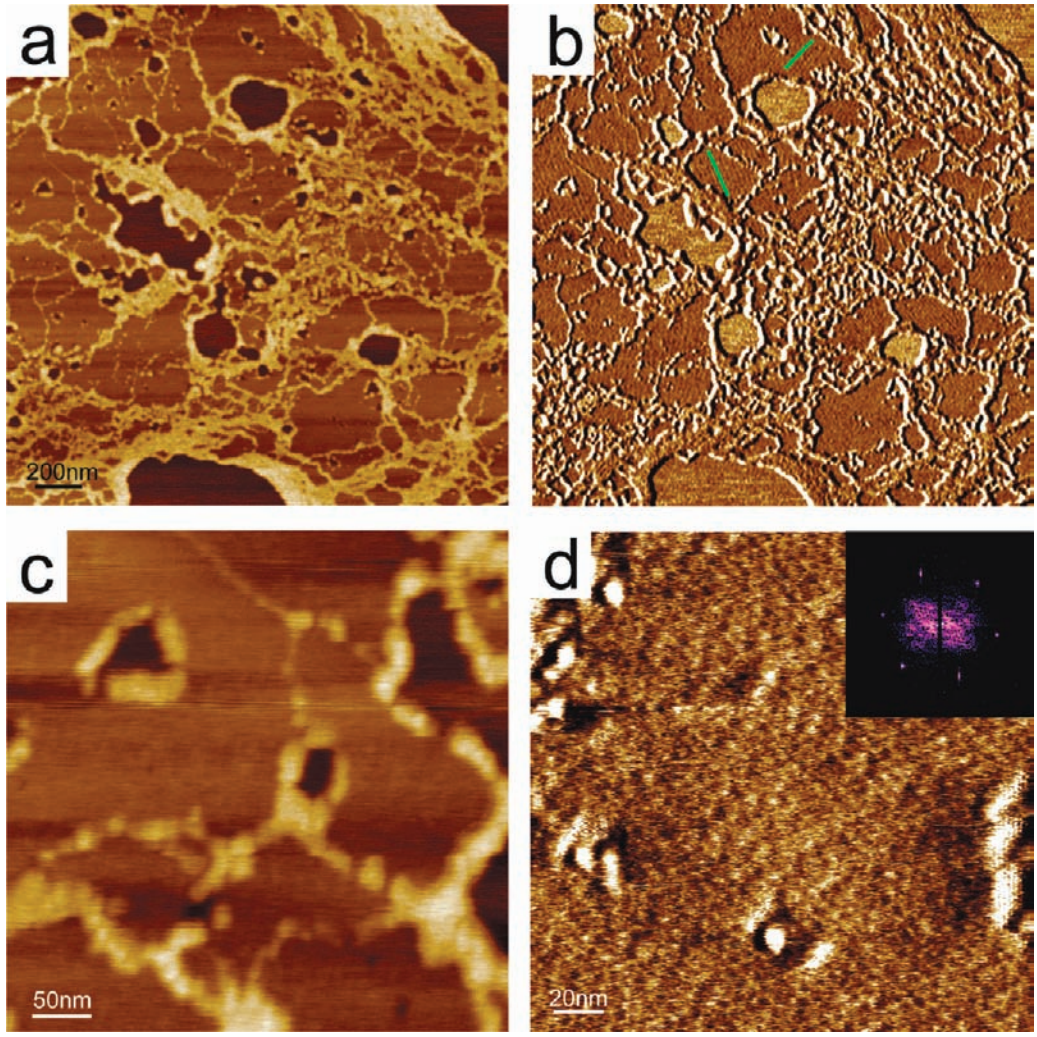

Figure 14. Large-scale (a) and high-resolution (c) height image of **3b** self-assembled from toluene on mica. The thickness of the film equals 0.6 and 2.5 nm for the lower and higher part, respectively. In the flatter and thinner part, even at large scale the corresponding phase image (b) reveals periodical features with different orientations (indicated with green lines). The high-resolution phase image (d) shows a hexagonal close packing of bright spots, which is highlighted in the 2D FFT (inset).

the hexadecyl side chains seem to prevent both stacking and a long-range ordering in the film (except for the layer in direct contact with the substrate). Surprisingly, the AFM results indicate that the hexadecyl-decorated wheel adopts the same packing on mica as on graphite at the level of the layer in direct contact with the substrate.

Because the synthesis and purification of the compounds evidently works without any limiting factors, upscaling efforts

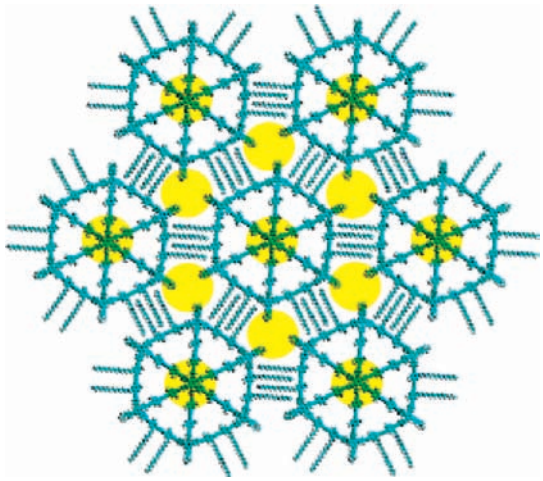

Figure 15. Schematic representation of the differences in repeating period of **3b** observed by STM and AFM. The yellow circles indicate those sites that most probably show up in the AFM images.

are envisaged, an important requirement for investigations of spoked wheels as rigid components in high-performance composite materials. Our current efforts are focused on the functionalization of the rim with branched side chains and dendrons to obtain meltable and/or mesomorphic derivatives.

Experimental Section

Synthesis. The syntheses of **1**, **2**, **4**, **6**, and **8** have been described previously,[23,37,38] while the syntheses of all new compounds are described in detail in the Supporting Information.

Dynamic Light Scattering. DLS measurements were carried out at 20 °C on an ALV CGS-3 goniometer using a HeNe laser ($\lambda = 632.8$ nm) and an ALV LSE-5004 correlator. Sample solutions (1 g L^{-1}, 1.0×10^{-4} mol L^{-1}, and 0.6×10^{-4} mol L^{-1}, respectively) were filtrated into a dust-free vial through a 0.45 μm hydrophobic PTFE filter. The correlation curve was fitted in a data point interval of 10−150 using the default DLS exponential $g_2(t)$ fit function with a target *PROB1* parameter of 0.5. The following solvent data (20 °C) were also used for the solutions by approximation:[73] $CHCl_3$ ($n^D_{20} = 1.4459$; $\eta = 0.58$ mPa s), toluene ($n^D_{20} = 1.4961$; $\eta = 0.59$ mPa s), cyclohexane ($n^D_{20} = 1.4266$; $\eta = 1.00$ mPa s).

Time-Resolved Fluorescence. Fluorescence lifetime and polarization anisotropy measurements of these systems were carried out in dilute solutions (0.3 mg L^{-1} concentration in $CHCl_3$) using a Hamamatsu streak camera with 2 ps time resolution under excitation by a 80 MHz repetition rate, frequency-doubled Ti:Sapphire laser at 370 nm.

Scanning Tunneling Microscopy. All experiments were carried out at 20−24 °C. Experiments were performed using a PicoSPM microscope (Agilent). Tips were mechanically cut from Pt−Ir wire (80:20 alloy, diameter 0.25 mm). Prior to imaging, **3a** and **3b** were dissolved in 1-phenyloctane, and a drop of the solution was applied onto a freshly cleaved surface of graphite (grade ZYB, Advanced Ceramics Inc., Cleveland, OH). The STM investigations were then performed at the liquid/solid interface within 1.5 h from dropcasting the solution. The graphite lattice was recorded by lowering the bias immediately after obtaining images of the 2D structure. The drift was corrected using this graphite lattice in the Scanning Probe Image Processor (SPIP) software (Image Metrology ApS).

Atomic Force Microscopy. The samples were dissolved in toluene at a concentration of less than 1 mg/g, and one droplet of the solution was then deposited on freshly cleaved HOPG or mica. After the solvent was completely evaporated (after at least several hours), the sample was characterized by AFM operating in intermittent contact mode. The AFM experiments were performed with a Nanoscope IV instrument using a *J* scanner.

Acknowledgment. This Article is dedicated to Prof. Gerhard Wegner on the occasion of his 70th birthday. Financial support by the Deutsche Forschungsgemeinschaft (DFG), the SFB 624, the VolkswagenStiftung, the K.U. Leuven (GOA), the Fund for Scientific Research - Flanders (F.W.O.), and the Belgian Federal Science Policy Office through IAP-6/27 is gratefully acknowledged. J.M.L. is a David and Lucile Packard Foundation Fellow.

Supporting Information Available: Further details on the recycling GPC separation, optical properties, and liquid crystallinity of **3b**, as well as full ^{1}H NMR, ^{13}C NMR, and MS spectra of **3a**, **3b**, **4**, **9b**, **10a**, **12a**, and **12b**, plus the synthetic procedures of all compounds not described previously by our groups. This material is available free of charge via the Internet at http://pubs.acs.org.

JA909229Y

(73) Weast, R. C. *CRC Handbook of Chemistry and Physics*, 63rd ed.; CRC Press Inc.: Boca Raton, FL, 1982−1983.